Mesoporous bioactive glasses equipped with stimuli-responsive molecular gates for the controlled delivery of levofloxacin against bacteria

Lorena Polo,[a,b] Natividad Gómez-Cerezo,[c,b] Alba García-Fernández,[a,c,d] Elena Aznar,[a,b,d] José-Luis Vivancos,[a,b,d,e] Daniel Arcos,[c,b] María Vallet-Regí,[c,b] and Ramón Martínez-Máñez*[a,b,d,e]

Abstract: Increase of bone diseases incidence has boosted the study of ceramic biomaterials as a potential osteo-inductive scaffolds. Particularly, mesoporous bioactive glasses have demonstrated to possess a broad application in the bone regeneration field, due their osteo-regenerative capability and their ability to release drugs from its mesoporous structure. These special features have been studied as an option to fight against bone infection, which is one of the most common problems regarding bone regeneration therapies. In this work, we develop a mesoporous bioglass functionalized with polyamines and capped with ATP as molecular gate for the controlled release of the antibiotic levofloxacin. Phosphate bonds of the ATP are hydrolyzed in the presence of acid phosphatase (APase), which significantly increases its concentration in bone infection due to the activation of bone resorption processes. The solid has been characterized and tested successfully against bacteria. The final gated solid only induces bacterial death in the presence of acid phosphatase. Additionally, it has also been demonstrated that the solid is not toxic for human cells. The double function of the prepared nanodevice as drug delivery system and bone regeneration enhancer, confirms the possible development of a new approach in tissue engineering field, where controlled release of therapeutic agents can be finely tuned at the same time that osteoinduction is favoured.

[a] L. Polo, A. García-Fernández, Dr. E. Aznar, Dr. J.L. Vivancos, Prof. R. Martínez-Máñez
Instituto Interuniversitario de Investigación de Reconocimiento Molecular y Desarrollo Tecnológico (IDM), Universitat Politècnica de València, Universitat de València
Camino de Vera s/n, 46022, Valencia, Spain.
E-mail: rmaez@qim.upv.es

[b] L. Polo, N. Gómez-Cerezo, A. García-Fernández, Dr. E. Aznar, Dr. J.L. Vivancos, Dr. D. Arcos, Prof. M. Vallet-Regí, Prof. R. Martínez-Máñez.
CIBER de Bioingeniería Biomateriales y Nanomedicina (CIBER-BBN), Spain.

[c] N. Gómez-Cerezo, Dr. D. Arcos, Prof. M. Vallet-Regí.
Departamento de Química en Ciencias Farmacéuticas (Química Inorgánica y Bioinorgánica)
Facultad de Farmacia
Universidad Complutense de Madrid, Plaza Ramón y Cajal s/n 28040, Madrid, Spain.

[d] A. García-Fernández, Dr. E. Aznar, Dr. J.L. Vivancos, Prof. R. Martínez-Máñez.
Unidad Mixta UPV-CIPF de Investigación en Mecanismos de Enfermedades y Nanomedicina, Universitat Politècnica de València, Centro de Investigación Príncipe Felipe, Valencia, Spain.

[e] Dr. J.L. Vivancos, Prof. R. Martínez-Máñez.
Unidad Mixta de Investigación en Nanomedicina y Sensores.
Universitat Politècnica de València, Instituto de Investigación Sanitaria La Fe, Valencia, Spain.

Supporting information for this article is given via a link at the end of the document.

Introduction

Bone diseases have gained importance over the last years due to the ageing of population. Incidence of illnesses like osteoporosis, bone tumours and bone fractures is remarkably higher in elderly patients, due to age-related loss and weakening of bone tissue.[1] Treatment of these kind of diseases usually implies the use of implants and bone prosthesis; however, surgical procedures are not always infallible, since they can result in other medical complications.[2,3] Currently, bacterial infection is one of the most frequent problems related to implant surgery.[4] The creation of a bacterial biofilms on the surface of the implant requires many times its removal and leads to healing difficulties, lowering the life-quality of patients.[5] Therefore, the need of new therapies and devices for the treatment of these diseases has led to arise the development of innovative biomaterials for bone tissue engineering.[6,7] Among them, mesoporous bioactive glasses are promising and innovative silica-based bioceramics which have a meaningful significance in bone tissue engineering field due to their excellent properties.[8–10] These materials are biocompatible and resorbable, and are able to integrate living bone in a physiological environment through the formation of hydroxyapatite on the surface of the implant.[11,12] This apatite-like phase is very similar to the inorganic component of the bones, and its enhanced formation in bone defects greatly favours bone regeneration.[13] These features make mesoporous bioactive glasses ideal materials for bone grafting and bone regeneration therapies. Apart from that, their mesoporous structure gives them special surface features,[14] and converts them suitable for drug delivery of certain substances.[15,16]

Several studies have reported the storage and release of different therapeutic drugs in order to treat local bone pathologies.[17] However, these examples are in most cases

based on sustained release processes which are not able to avoid unspecific release. Taking into account these precedents, it is of interest the development of more sophisticated systems able to promote bone regeneration and achieve controlled drug delivery only in specific scenarios. Various nanostructured systems have been recently designed for the controlled release of anticancer and antiviral drugs.[18,19] Moreover, the preparation of new drug nanocarriers able to respond to external stimuli to perform a controlled and local cargo release has been of enormous importance in the field of biomedicine.[20,21] In this context, one appealing approach to succeed in this goal is the incorporation of molecular gates to mesoporous bioglasses. A molecular gate is a molecular or supramolecular-based system able to control mass transport and respond to specific external stimuli which can be implemented in a porous scaffold.[22,23] Different gated materials using molecules, biomolecules or supramolecules have been described. In these examples, the gating mechanism can be switched between a "closed" to "open" state, or vice versa, by the application of a selected stimulus as light,[24] temperature,[25,26] magnetic fields,[27] ultrasounds,[28] pH changes,[29] redox reactions[30] or biomolecules as enzymes.[31-24] Molecular gates have been widely studied and incorporated in mesoporous silica supports,[35] but very rarely have been implemented in mesoporous bioglasses.[36] Despite the relevance of combining the osteoinductive features of mesoporous bioactive glasses and controlled release characteristics of molecular gates, much effort in the development of this kind of functional biomaterials should still be accomplished and applied to a relevant context. In this scenario, the aim of this work is the development of a gated system able to respond specifically to the presence of a stimulus related with bone infection.

For this purpose, an 80%SiO_2-15%CaO-5%P_2O_5 (% mol) mesoporous bioglass was selected as inorganic support (**S1**). This solid was loaded with levofloxacin, which is a wide range antibiotic, and functionalized with 3-[2-(2-aminoethylamino)ethylamino]propyl-trimethoxysilane. The resulting solid (**S2**) was treated with ATP (Adenosine 5′-triphosphate disodium salt hydrate) and EDC, in order to covalently attach the phosphate group in ATP with the amine in **N3** (solid **S3**). In this way, ATP molecules were grafted to the surface of the solid, blocking the entrance to the mesopores and keeping the cargo in the pore voids. In a non-pathological scenario, ATP molecules would remain intact, and levofloxacin would continue stored inside the pores of the mesoporous bioactive glasses. However, in the presence of a stimulus as acid phosphatase (APase), ATP molecules would be hydrolysed, unblocking the surface of the pores and allowing the release of the drug. This mechanism has been previously used by the present authors to develop gated 3D scaffolds and as intracellular drug delivery system.[37,35] APase was selected as stimulus since its concentration significantly increases with osteoclast activity.[38,39] Both osteoblast deposition and osteoclast resorption are two balanced processes which are fundamental for bone regeneration.[40] However, the presence of infectious microorganisms as *Staphylococcus aureus* can enhance osteoclast resorption and lead into bone damage with the subsequent increase of acid phosphatase levels.[41] The action mechanism of phosphatase enzymes consists of the cleavage of phosphate bonds. Thus, in a bone infection scenario ATP molecules would be cleaved, unblocking the entrance to the mesopores of the MBG and allowing the release of the drug to the media (**Scheme 1**).

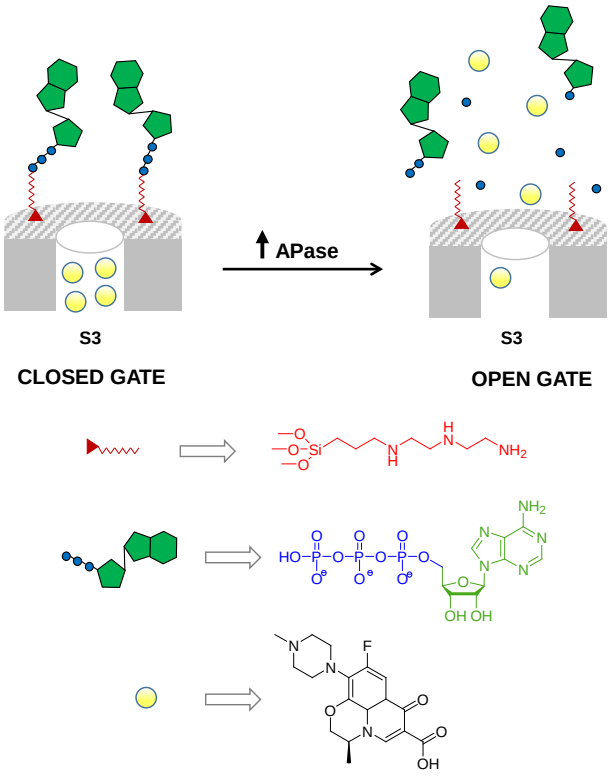

Scheme 1. Schematic representation of solid **S3** capped with the ATP molecular gates.

The resulting solid (**S3**) was characterized, to assure that the functionalization process did not modify the properties of the support. Controlled release tests were carried out both in the presence and the absence of acid phosphatase, achieving drug release only in the presence of the stimulus. Bioactivity assays were carried out with gated and non-gated solids, to demonstrate that the molecular gates do not slow down bioactive processes. Moreover, bacterial death experiments were carried out in order to confirm the antibacterial activity of the solid in a specific scenario. Finally, cytotoxicity assays were carried out with the gated solid to assess that the solid is not toxic for human cells.

Results and Discussion

The aim of this work was the development of a gated bioglas able to deliver an antibiotic (levofloxacin) in the presence of a stimulus (presence of APase) related with bone infection. For this, a mesoporous bioactive glass (solid **S1**) was loaded with levofloxacin and then functionalized first with **N3** and then with ATP to yield solids **S2** and **S3**, respectively. The synthesized solids were correspondingly characterized in order to confirm the presence of the ATP gates, and to demonstrate that the mesoporous properties of the final solid **S3** had not been damaged upon the functionalization and capping processes. Thus, chemical, structural and textural characterization was carried out in solids **S1**, **S2** and **S3**. The highly ordered mesoporous structure of the solids was confirmed by powder X-ray diffraction (XRD). XRD pattern for **S1** (**Figure 1**) shows a single peak at 1.71 ° that corresponds to a (10) Bragg reflection of a 2D hexagonal p6m structure. **S2** and **S3** show similar peaks. Peaks intensity decreases after the loading and capping process, pointing out the introduction of certain degree of disorder with these processes.

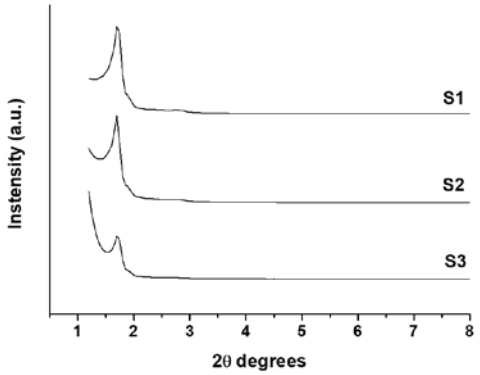

Figure 1. Powder X-ray diffraction patterns of solids **S1**, **S2** and **S3.**

Transmission electron microscopy studies were also carried out in order to confirm XRD results. TEM image of **S1** evidences mesoporous structure, showing alternate black and white stripes typical of p6m hexagonal pore symmetry (**Figure 2**). TEM images of **S2** and **S3** show that mesoporous structure of the solids was not affected during the loading, functionalization and capping processes.

Textural properties of the prepared materials were characterized by N_2 adsorption-desorption studies. The N_2 adsorption-desorption isotherm of **S1** shows a curve of type IV, typical of mesoporous solids (**Figure 3**). The curve shows an adsorption step between P/P_0 0.4 and 0.6, due to N_2 condensation inside pores. Moreover, the curve has a H1 hysteresis loop also typical of mesoporous materials, which indicates that mesopores have open cylinder morphology. N_2 adsorption-desorption isotherm of **S3** shows a decrease of BET surface and specific pore volume when compared with **S1**, due to the loading of the pores

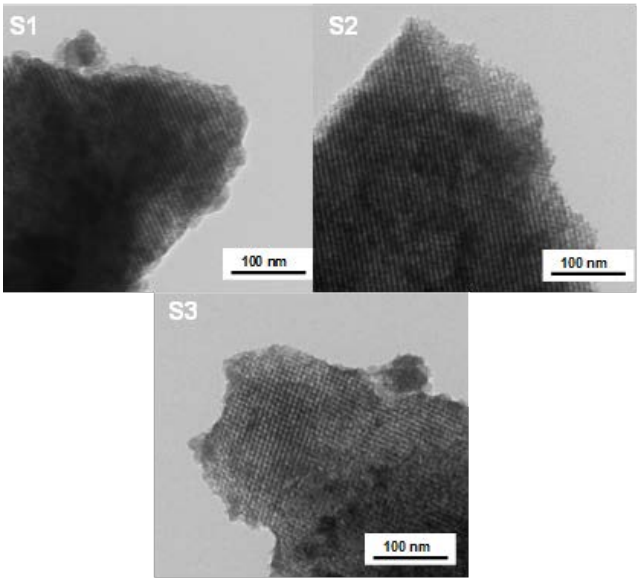

Figure 2. Transmission electron microscope images of solids **S1**, **S2** and **S3**.

and grafting of ATP. The hysteresis loop of the curve for **S3** changes to type H2 when compared with that of **S1**, which means that the morphology of the pore has also changed, indicating an ink-bottle shape according to the capping of the material. Finally, pore size distribution was determined from the adsorption branch of the isotherm by means of the Barret-Joyner-Halenda (BJH) method and the surface area was determined using the Brunauer-Emmett-Teller (BET) method. Textural parameters values of **S1** and **S3** are summarized in **Table 1**.

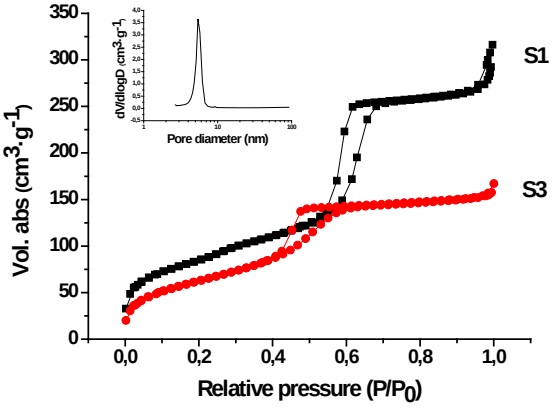

Figure 3. N_2 adsorption-desorption isotherms for solids **S1** and **S3.**

Moreover, thermogravimetric analysis was performed in solid **S3** to determine the amount of N3 and ATP attached to the surface of the material. Results are shown in **Table 2**. Moreover, the amount of levofloxacin contained into the pores was determined. For this, 10 mg of solid **S3** were treated with APase and the solid allowed to release the

cargo for 24 hours. From a fluorescence calibration curve, it was determined that the amount of levofloxacin was 2.53 mg per gram of **S3**.

Table 1. Textural parameters of solids **S1** and **S3**.

Solid	BET surface ($m^2 \cdot g^{-1}$)	Pore Volume ($cm^3 \cdot g^{-1}$)	Pore size (nm)
S1	305.50	0.386	5.5
S3	233.98	0.210	3.9

Table 2. Organic content (α, mg/g of solid) in solid **S3**.

Solid	α_{levo}	α_{N3}	α_{ATP}
S3	2.53	179.8	22.97

As previously stated, the designed nanodevice is based on the combination of a biocompatible material and a gating mechanism to induce apatite-like formation and control drug release at the same time. For this reason, both bioactivity and drug delivery assays were carried out with solid **S3**. In order to demonstrate that the ATP-capped solid is capable to release the payload only in specific scenarios, drug delivery studies were undertaken in the presence and the absence of acid phosphatase. In a typical experiment, 2 mg of **S3** were suspended in water at pH 7.6 and stirred for 24 hours in the presence and the absence of the stimulus. At given time intervals, fractions of both suspensions were taken and filtrated to remove the solid. Then, drug released from the pore voids was monitored by fluorescence spectroscopy (λ_{ex} 292 nm, λ_{em} 494 nm). Drug delivery kinetics is shown in **Figure 4**. In the absence of stimulus, the solid showed poor release, (less than 20 % of the maximum cargo delivered). Contrarily, in the presence of acid phosphatase, a remarkable payload of the drug was achieved, reaching maximum delivery at 24 hours. These results are consistent with the design of the nanodevice. In the absence of APase, the ATP gates remain closed, blocking the entrance to the pores and avoiding levofloxacin leakage. When acid phosphatase is added the phosphate bonds in ATP are hydrolysed, pore entrances are unblocked and levofloxacin is released.

In order to demonstrate that gate opening was caused by the presence of APase, controlled release experiments were carried out in the presence of other enzymes as amylase and lipase. Delivery kinetics of this experiment are shown in **Figure 4** and demonstrate that the presence of other enzymes did not induce cargo delivery.

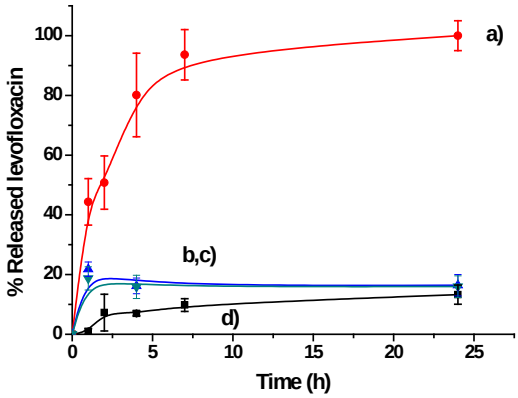

Figure 4. Delivery kinetics of solid **S3** in the presence of acid phosphatase (a), amylase (b) and lipase (c), and in the absence of acid phosphatase (d).

Additionally, levofloxacin kinetics release can be explained by using the Higuchi model.[42,43] This simple model, used for similar systems,[44] predicts that the release of the cargo will be dependent on the square root of time when delivery is based on a Fickian diffusion process. In this case, the amount of guest release, Qt, per unit of exposed area at time t can be described by the equation:

$$Q_t = k_H \, t^{1/2}$$

where k_H is the release rate constant for the Higuchi model. When applied to the experimental data, a good linear fitting was observed (see **Figure 5**) and a value of K_H of 35,836 was calculated. These data suggest that the delivery of levofloxacin from pores of solid **S3** is basically a diffusive process.

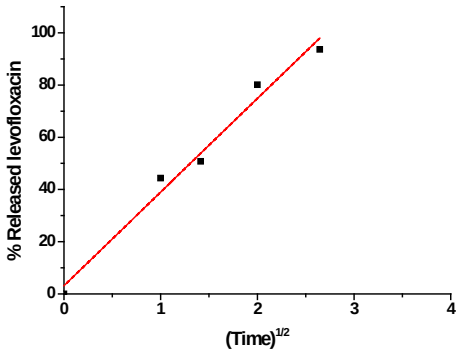

Figure 5. Delivery kinetics of solid **S3** versus the square root of time

Molecular gates provide to mesoporous bioactive glass the ability to perform controlled drug release, but also imply a certain modification of the bioactive glass surface. Therefore, we found important to check that the molecular gates did not harm the bioactive capability of the material. Thus, the bioactive behaviour of solid **S3** was studied by soaking the material in simulated body fluid (SBF) at 37 °C. As solid **S3** was meant to be bioactive in the presence of

acid phosphatase, the bioactivity test with **S3** was carried on in the absence and the presence of the enzyme in order to study the system with both, open and closed gates. Bioactivity of solids was studied by FTIR spectroscopy to identify the signals corresponding to the presence of phosphate bonds. In addition, field emission scanning microscopy images were taken with the purpose of confirming FTIR results, and EDX analysis was performed in order to study the components of the solids surface before and after soaking in SBF. FTIR spectra of **S3** in the presence and the absence of APase at 0 and 72 hours are shown in **Figure 6**. Non-soaked solid **S3** shows typical Si-O signal at 900-1250 cm^{-1}, and signal in 520-610 cm^{-1} corresponding to the presence of amorphous phosphate bonds. Moreover, amine δ(C-N) and δ(C-H) bands are observed at 1470 cm-1 and 1650 cm-1. A typical weak amine δ(N-H) band is also observed at 3250 cm-1. The FTIR spectrum of **S3** after being soaked for 72 hours in the absence of APase remains unchanged. FTIR spectra of solid **S3** in the presence of acid phosphatase shows typical MBG signals and amine signals at 1470, 1650 and 3300 cm^{-1}, but a splitting of the signal at 560 and 600 cm^{-1} is also clearly observed after 24 and 72 hours of soaking. This splitting demonstrates the presence of P-O bonds corresponding to a crystalline phase, which is consistent with the formation of apatite.

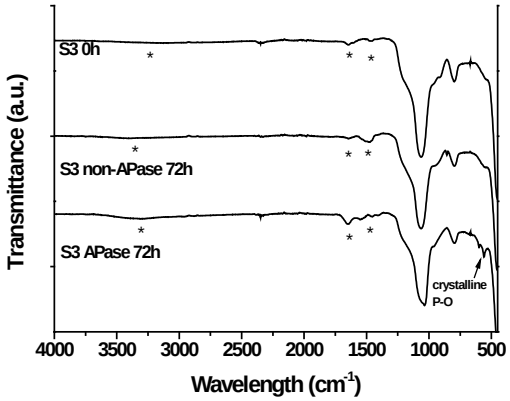

Figure 6. FTIR spectra of non-soaked **S3**, 72 hours soaked **S3** with no APase, and 72 hours soaked **S3** with APase.

In order to confirm the results given by FTIR spectroscopy, FESEM images of the different treated solids were taken, and EDX analysis was performed. Si, Ca and P percentages are shown in **Table 3**. Non-soaked solid **S3** showed a neat surface with no apatite (**Figure 7A**), and **S3** soaked for 72 hours in the absence of APase also presents the same neat surface, with low calcium and phosphor percentages (**Figure 7B**). Actually, for the later the amount of calcium decreases due to the release of Ca^{2+} ions from the mesoporous bioglass. Ca^{2+} release from the material also causes the rise of silicon percentage, while phosphorous amount slightly rises too. These results are

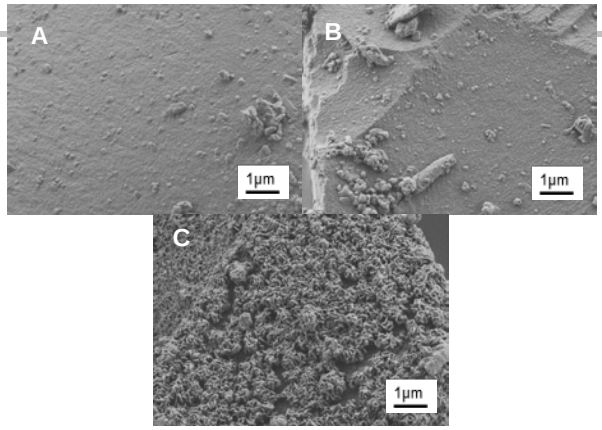

Figure 7. SEM images of non-soaked **S3** (A), 72 hours soaked **S3** with no APase (B), and 72 hours soaked **S3** with APase (C).

consistent with FTIR spectra, which show no crystalline P-O presence in **S3** containing the ATP molecular gates. However, when **S3** is soaked for 72 hours in the presence of acid phosphatase, a new thick phase is rapidly formed on the surface of the solid (**Figure 7C**). EDX analysis confirms the high amounts of calcium and phosphorous. Ratio Ca/P was found to be 1.46, which is in agreement with the presence of the apatite-like phase. These results are also consistent with FTIR spectra, demonstrating that the solid with “open gates” recovers its bioactive properties.

Table 3. EDX results of Si, Ca and P percentages in non-soaked **S3**, 72 hours soaked **S3** with no APase, and 72 hours soaked **S3** with APase.

%	S3 0h	S3 72h	S3-APase 72h
Si	85.37	90.03	75.66
Ca	11.13	6.01	14.46
P	3.50	3.96	9.88

The loss of bioactivity after the incorporation of the ATP molecular gates has not been deeply studied in this work. A hypothetical explanation to the non-bioactive behaviour of solid **S3** in the absence of acid phosphatase could be related to the ability of mesoporous bioglasses to release Ca^{2+} ions to the media. As stated in literature,[45] bioactive processes start with the Ca^{2+} leaking from the silica net and undergoing an exchange with H^{+} ions. In a physiological media, calcium ions are capable of reacting with phosphates to form a crystalline apatite layer. It has also been reported that phosphate groups have a high affinity for Ca^{2+} ions.[45] In this context, it is possible that the phosphate net formed by the ATP molecules could entrap Ca^{2+} ions, avoiding the leakage to the media and therefore inhibiting bioactive behaviour. Moreover, the breaking of the phosphate net would allow the entrapped calcium release, which is consistent with results of **S3** in the presence of acid phosphatase. Actually, the release of ATP molecules would rise phosphates concentration in the media, which could also favour the apatite phase formation.

Thus, solid **S3** was not bioactive when capped with ATP. However, once mimicked bacterial infection conditions (with

the subsequent increase of acid phosphatase in the media), the **S3** bioactivity was restored.

As solid **S3** was expected to release an antibiotic drug in the presence of an infection, bacterial viability assays were carried out with the purpose of demonstrating the bactericide effect of the nanomaterial. In a typical experiment **S3** was stirred at 37 °C in the absence and the presence of acid phosphatase for 24 hours. Then, two different *E.coli* suspensions were treated with 50 µL of each sample. Bacteria were stirred for 20 minutes and afterwards 100 µL of each suspension was seeded in an agar plate and incubated at 37 °C. After 24 hours, cell viability was quantified by counting the colonies. As seen in **Figure 8**, bacteria treated with the **S3** suspension (without APase) showed a viability of 80.41 %, which is remarkably higher than 18.75 % of viability when bacteria were treated with the **S3** suspension previously treated with APase. Decreased viability for the former compared with control (100 %) can be due to the residual release of levofloxacin in the absence of acid phosphatase. Moreover, bacteria were also treated with a solution containing only APase and no significant bacterial death was observed, demonstrating that the bacterial death was due to the presence of released levofloxacin (data not shown). These results are consistent with the design of the gated support **S3**. In the presence of acid phosphatase, the gated support delivers levofloxacin in a much higher amount that that in the absence of the stimulus. The higher concentration of drug in APase supernatant undertakes higher cell toxicity, demonstrating that the bactericide effect of the solid is only achievable in the presence of an infection marker as acid phosphatase.

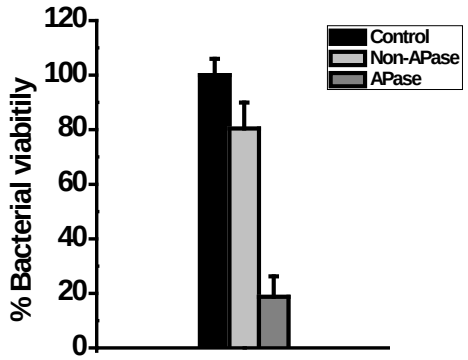

Figure 8. Bacterial viability of *E.coli* when treated with 50 and 100 µL of a suspension of **S3** in the presence and the absence of APase.

Finally, cytotoxicity studies were carried out in order to demonstrate that the prepared material is compatible with human cells. For this purpose, U-2 OS human osteosarcoma cells were treated with different amounts (25, 50, 100 and 200 µg·mL^{-1}) of **S3** for 24 and 48 hours, and mitochondrial activity (WST-1 assays) was measured after these intervals. As seen in **Figure 9**, **S3** solid was well-tolerated by U-2 OS cells at concentrations up to 200 µg·mL^{-1} after 24 and 48 hours of exposure, which means that the prepared solid is not toxic. Thus, it was demonstrated that the ATP-gated mesoporous bioactive glass is biocompatible, and is a good strategy to treat bone infection and improve bone regeneration without causing any damage to human cells.

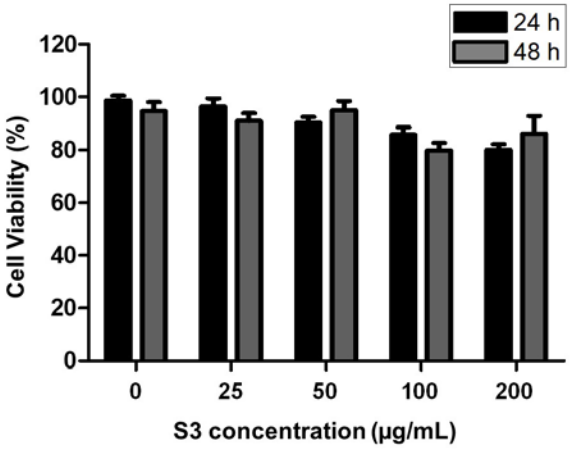

Figure 9. Cell viability of U-2 OS cells in the presence of **S3** (0, 25, 50, 100 and 200 µg·mL^{-1}) after 24 hours (black) and 48 hours (gray) of incubation. Three independent experiments containing triplicates were carried out. Data are expressed as mean ± s.e.

Conclusions

In summary, we have developed a double-strategy device which is able to enhance bone regeneration and achieve controlled drug release against bacteria. A mesoporous bioactive glass was loaded with levofloxacin, functionalized with a polyamine, and capped with ATP molecules. The structure of the resulting solids was characterized by standard techniques, demonstrating that the incorporation of molecular gates into MBG did not imply any changes in its textural properties. Then, both drug release capability and bioactive behaviour were tested. Drug release experiments were carried out with the final solid in the presence and the absence of acid phosphatase, and also in the presence of other enzymes as amylase and lipase, observing only a complete release of the drug when acid phosphatase was present. This demonstrates that controlled release is achieved only in the presence of a specific stimulus typical of a bone infection environment. On the other hand, bioactivity studies were carried out with **S3** in the presence and the absence of acid phosphatase. Our studies proved that the solid did not have bioactive capabilities when capped with ATP gates, however, it was found that the solid recovered its bioactive behaviour in the presence of the acid phosphatase stimulus. Antibacterial effect of **S3** was also studied, and it was demonstrated that solid treated with acid phosphatase was much more effective killing bacteria than the untreated solid. Finally,

cytotoxicity studies were carried out with **S3**, showing that the prepared material was not toxic for U-2 OS human cells upon 24 and 48 hours. In this way, our double-strategy design has been proved to be successful as a drug delivery system and bone regeneration enhancer. The present work confirms the versatility of the used gating mechanism previously applied to the development of 3D scaffolds and as intracellular drug delivery system. This kind of double-edged nanodispositives opens up a new approach in tissue engineering field, particularly in the treatment of osseous diseases as bone infection.

Experimental Section

Chemicals

Chemicals poly(ethylene glycol)-block-poly(propylene glycol)-block-poly(ethylene glycol) (P123), tetraethyl orthosilicate (TEOS), triethyl phosphate (TEP), calcium nitrate $Ca(NO_3)2{\cdot}4H_2O$, 3-[2-(2-aminoethylamino)ethylamino]propyl-trimethoxysilane (N3), adenosine 5'-triphosphate disodium salt hydrate (ATP), N-(3-dimethylaminopropyl)-N'-ethylcarbodiimide hydrochloride (EDC), acid phosphatase, acetonitrile anhydrous, hydrochloric acid, levofloxacin, Dulbecco's Modified Eagle's Medium (DMEM), fetal bovine serum (FBS) and Dulbecco's phosphate-buffered saline (PBS) were purchased from Sigma–Aldrich Química S.A. LB medium was provided from Laboratorios Conda. Cell proliferation reagent WST-1 was obtained from Roche Applied Science.

General Techniques

FTIR spectroscopy was carried out with a Tensor 27 FT-IR spectrometer (Bruker). TEM images were obtained with a 100 kV Jeol JEM-1010 microscope. FESEM images were obtained with a ZEISS ULTRA 55. Powder X-ray diffraction measurements were performed on a Philips D8 Advance diffractometer using Cu Kα radiation. Textural properties of the calcined materials were determined by nitrogen adsorption porosimetry by using a Micromeritics TriStar II PLUS porosimeter. To perform the N_2 adsorption measurements, the samples were previously degassed under vacuum for 24 hours, at 90 °C. Surface area was determined using the Brunauer-Emmett-Teller (BET) method.[46] Pore size distribution between 0.5 and 40 nm was determined from the adsorption branch of the isotherm by means of the Barret-Joyner-Halenda (BJH) method.[47] For cell proliferation test, cell viability measurements were taken in a Wallac 1420 workstation. Thermogravimetric analysis were carried out on a TGA/SDTA 851e Mettler Toledo balance, using an oxidant atmosphere (air, 80 mL/min) with a heating program consisting on a heating ramp of 10 ºC per minute from 393 to 1273 K and an isothermal heating step at this temperature during 30 minutes.

Synthesis of materials

Synthesis of mesoporous bioactive glass (S1). 80%SiO_2-15%CaO-5%P_2O_5 (% mol) mesoporous glass (**S1**) was synthetized by evaporation induced self-assembly (EISA) method, using P123 triblock copolymer as structure directing agent. TEOS, TEP and calcium nitrate $Ca(NO_3)_2{\cdot}4H_2O$ were used as SiO_2, P_2O_5 and CaO sources respectively. In a typical synthesis, 4 g of P123 were dissolved in 60 g of ethanol with 1 mL of HCl 0.5 M solution at room temperature. Afterwards, 7.18 mL of TEOS, 0.73 mL of TEP and 1.29 g of $Ca(NO_3)_2{\cdot}4H_2O$ were added under stirring in 3 hours intervals. The resulting solution was stirred for 12 hours and casted into Petri dishes (9 cm in diameter). The colourless solution was evaporated at 37 °C for 1 day. Eventually, the dried gels were removed as homogeneous and transparent membranes and heated at 700 °C for 3 hours under air atmosphere. Finally, the MBG powder was gently milled and sieved, collecting the particle size fraction below 20 μm.

Synthesis of S2. 500 mg of **S1** were suspended in a solution of 145 mg of levofloxacin in 20 mL of anhydrous acetonitrile under inert atmosphere. After stirring for 24 hours in order to achieve the maximum pore loading, 0.5 mL of 3-[2-(2 aminoethylamino)ethylamino] propyl-trimethoxysilane (**N3**) was added, and the mixture was stirred for 5.5 hours. Finally, the solid was filtered and dried under vacuum. Following this procedure, the levofloxacin spectrum does not change before and after loading into the mesoporous bioglass.

Synthesis of S3. 400 mg of solid **S2** were suspended in a solution containing EDC 0.6 M, ATP 0.5 M and an excess of levofloxacin. The pH of the solution was previously adjusted to 7.6 with NaOH. The suspension was stirred for 6 hours at room temperature. The resulting solid was filtered and dried under vacuum.

Stimuli-responsive studies with S3

4 mg of **S3** were suspended in 10 mL of water at pH 7.6 adjusted with NaOH. The suspension was divided in two, and acid phosphatase (2.5 mg, 1.25 enzymatic units) was added to one of the samples. Both samples were stirred at 400 rpm and 37 °C, and then several 250 μL aliquots were taken for each sample at different times (0, 1, 2, 4, 7 and 24 hours). These aliquots were filtered with PTFE filters (0.22 μm) to monitor the levofloxacin release by fluorescence spectroscopy (λ_{ex} 292 nm, λ_{em} 494 nm). Moreover, the same experiment was performed in the presence of other enzymes as amylase and lipase, and in the presence of denatured APase. For this, 10 mg of **S3** were suspended in 25 mL of water at pH 7.6 and the suspension was divided in five samples. APase, denatured APase, lipase and amylase (7.5 enzymatic units) were added to respective samples. The samples were stirred at 400 rpm and 37 °C, and then 250 μL aliquots were taken for each sample at different times. These aliquots were filtered with PTFE filters (0.22 μm) to monitor the levofloxacin release by fluorescence spectroscopy (λ_{ex} 292 nm, λ_{em} 494 nm).

Bioactivity assays with S1 and S3.

In vitro bioactivity assays were carried out on **S1** and **S3** solids. 10 mg of each solid were soaked into 2 mL of filtered simulated body fluid (SBF)[35] at 37 °C under sterile conditions. The evolution of the solids surfaces were analysed by Fourier transform infrared (FTIR) spectroscopy and field emission scanning electron microscopy (FESEM).

Bacterial viability assay

***E. coli* DH5α culture conditions.** For bacterial viability studies, *Escherichia coli (E.coli)* DH5α cell culture was used. Bacteria cells were maintained in glycerol 15 % at -80 °C. For the assays, cells were grown for 24 hours at 37 °C and under constant stirring with 5 mL of LB medium. Cells from 1 mL of culture were collected by centrifugation for 30 seconds at 13000 rpm and resuspended in 1 mL of milliQ water at pH 7.6.

Bacterial viability assay. In order to determine the antibacterial effect of **S3**, 5 mg of the solid were stirred in water at pH 7.6 in the absence and the presence of acid phosphatase for 24 hours. Then, two suspensions of 10^4 cells·mL^{-1} were prepared and treated with 50 µL of each sample. A control experiment with no solid was also carried out. The suspensions were stirred at 180 rpm (37 °C) during 10 minutes. Then, they were suitably diluted with milliQ water (pH 7.6) in order to obtain a cell growth easy to quantify. Finally, 100 µL of the new dilutions were seeded in LB plates (3 % agar) and incubated at 37 °C for 24 hours. Then, Colony Formation Units (CFU) were quantified.

Citotoxicity assay

Cell culture conditions

U-2-OS human osteosarcoma cells were purchased from ATCC and were grown in DMEM supplemented with 10 % of FBS. Cells were incubated at 37 °C in an atmosphere of 5 % carbon dioxide and 95 % air and underwent passage twice a week.

Cell toxicity assay. In order to study viability of cells in contact with **S3**, U-2-OS cells were seeded in a 96-well plate in a density of 10.000 cells·well^{-1} and treated with 25, 50, 100 and 200 µg·mL^{-1} of **S3** in PBS. A control assay with no solid was also carried out. After 24 and 48 hours of incubation, WST-1 was added in order to determine cell viability. Cells were incubated for 60 minutes, and then absorbance was measured at 595 nm.

Statistics

Statistics Data are expressed as means-standard deviations of experiments. Statistical analysis was performed using the Statistical Package for the Social Sciences (SPSS) version 22 software (IBM). Statistical comparisons were made by analysis of variance (ANOVA). In all of the statistical evaluations, P<0.01 was considered as statistically significant.

Acknowledgements

The authors thank the Spanish Government for projects MAT2015–64139-C04–01-R, MAT2015-64831-R, MAT2016-75611-R (AEI/FEDER, UE). Also, Generalitat Valenciana (project PROMETEOII/2014/047) and CIBER-BBN (project SPRING) are acknowledged for their support. M.V.-R. acknowledges funding from the European Research Council (Advanced Grant VERDI; ERC-2015-AdG Proposal 694160). L.P. thanks Universitat Politècnica de València for her FPI grant. N. G. C. and A. G thank to Ministerio de Ciencia e Innovación and Ministerio de Educación, Cultura y Deporte for their predoctoral fellowships. The authors also thank the Electron Microscopy Service at the UPV for their support.

Keywords: nanomaterials, controlled release, mesoporous bioactive glasses.

[1] R. Bernabei, A. M. Martone, E. Ortolani, F. Landi, E. Marzetti, *Clin. Cases Miner. Bone Metab.* **2014**, *11*, 201–7.

[2] J. Li, H. L. Wang, *Implant Dent.* **2008**, *17*, 389–401.

[3] A. S. Herford, J. S. Dean, *Oral Maxillofac. Surg. Clin. North Am.* **2011**, *23*, 433–442.

[4] C. R. Arciola, L. Visai, F. Testoni, S. Arciola, D. Campoccia, P. Speziale, L. Montanaro, *Int. J. Artif. Organs* **2011**, *34*, 771–780.

[5] J. A. Inzana, E. M. Schwarz, S. L. Kates, H. A. Awad, *Bone* **2015**, *72*, 128–136.

[6] L.-C. Gerhardt, A. R. Boccaccini, *Materials (Basel).* **2010**, *3*, 3867–3910.

[7] F. Baino, G. Novajra, C. Vitale-Brovarone, *Front. Bioeng. Biotechnol.* **2015**, *3*, 202.

[8] L. L. Hench, *Science (80-.).* **1980**, *208*, 826–831.

[9] C. Argyo, V. Weiss, C. Bräuchle, T. Bein, *Chem. Mater.* **2014**, *26*, 435–451.

[10] X. X. Yan, H. X. Deng, X. H. Huang, G. Q. Lu, S. Z. Qiao, D. Y. Zhao, C. Z. Yu, *J. Non. Cryst. Solids* **2005**, *351*, 3209–3217.

[11] X. Yan, C. Yu, X. Zhou, J. Tang, D. Zhao, *Angew. Chemie - Int. Ed.* **2004**, *43*, 5980–5984.

[12] N. Gómez-Cerezo, I. Izquierdo-Barba, D. Arcos, M. Vallet-Regí, *J. Mater. Chem. B* **2015**, 3810–3819.

[13] L. L. Hench, R. J. Splinter, W. C. Allen, T. K. Greenlee, *J. Biomed. Mater. Res.* **1971**, *5*, 117–141.

[14] J. R. Jones, *J. Eur. Ceram. Soc.* **2009**, *29*, 1275–1281.

[15] M. Manzano, M. Vallet-Regí, *J. Mater. Chem.* **2010**, *20*, 5593–5604.

[16] M. Vallet-Regí, D. Arcos, *Acta Mater.* **2013**, *61*, 890–911.

[17] Y. Zhu, S. Kaskel, *Microporous Mesoporous Mater.* **2009**, *118*, 176–182.

[18] D. Lembo, M. Donalisio, A. Civra, M. Argenziano, R. Cavalli, *Exp. Opin. Drug Deliv.* **2018**, *15*, 93-114.

[19] W. Chen, J. Ouyang, H. Liu, M. Chen, K. Zeng, J. Sheng, Z. Liu, Y. Han, L. Wang, J. Li, L. Deng, Y-N. Liu, S. Guo, *Adv. Mater.*, **2017**, *29*, 1603864.

[20] B.L. Li, M. I. Setyawati, L. Chen, J. Xie, K. Ariga, C.-T. Lim, S. Garaj, D. T. Leong, *ACS Appl. Mater. Interfaces*, **2017**, *9*, 15286-15296.

[21] M. Komiyama, K. Yoshimoto, M. Sisido, K. Ariga, *Bull. Chem. Soc. Jpn.* **2017**, *90*, 967-1004.

[22] E. Aznar, M. Oroval, L. Pascual, J. R. Murguía, R. Martínez-Máñez, F. Sancenón, *Chem. Rev.* **2016**, *116*, 561–718.

[23] E. Aznar, C. Coll, M. Dolores Marcos, R. M. Artínez-M Áñez, F. Sancenón, J. Soto, P. Amorós, J. Cano, E. Ruiz, *Chem. - A Eur. J.* **2009**, *15*, 6877–6888.

[24] J. L. Vivero-Escoto, I. I. Slowing, C.-W. Wu, V. S.-Y. Lin, *J. Am. Chem. Soc.* **2009**, *131*, 3462–3463.

[25] J. T. Sun, Z. Q. Yu, C. Y. Hong, C. Y. Pan, *Macromol. Rapid Commun.* **2012**, *33*, 811–818.

[26] A. López-Noriega, E. Ruiz-Hernández, E. Quinlan, G. Storm, W. E. Hennink, F. J. O'Brien, *J. Control. Release* **2014**, *187*, 158–166.

[27] E. Bringas, Ö. Köysüren, D. V. Quach, M. Mahmoudi, E. Aznar, J. D. Roehling, M. D. Marcos, R. Martínez-Máñez, P. Stroeve, *Chem. Commun.* **2012**, *48*, 5647.

[28] H. J. Kim, H. Matsuda, H. Zhou, I. Honma, *Adv. Mater.* **2006**, *18*, 3083–3088.

[29] L. Tan, M. Y. Yang, H. X. Wu, Z. W. Tang, J. Y. Xiao, C. J. Liu, R. X. Zhuo, *ACS Appl. Mater. Interfaces* **2015**, *7*, 6310–6316.

[30] Z. Zhang, D. Balogh, F. Wang, R. Tel-Vered, N. Levy, S. Y. Sung, R. Nechushtai, I. Willner, *J. Mater. Chem. B* **2013**, *1*, 3159–3166.

[31] C. De La Torre, I. Casanova, G. Acosta, C. Coll, M. J. Moreno, F. Albericio, E. Aznar, R. Mangues, M. Royo, F. Sancenón, et al., *Adv. Funct. Mater.* **2015**, *25*, 687–695.

[28] I. Candel, E. Aznar, L. Mondragón, C. de la Torre, R. Martínez-Máñez, F. Sancenón, M. D. Marcos, P. Amorós, C. Guillem, E. Pérez-Payá, et al., *Nanoscale* **2012**, *4*, 7237.

[32] A. Agostini, L. Mondragón, A. Bernardos, R. Martínez-Máñez, M. Dolores Marcos, F. Sancenón, J. Soto, A. Costero, C. Manguan-García, R. Perona, et al., *Angew. Chemie - Int. Ed.* **2012**, *51*, 10556–10560.

[33] M. Oroval, E. Climent, C. Coll, R. Eritja, A. Aviñó, M. D. Marcos, F. Sancenón, R. Martínez-Máñez, P. Amorós, *Chem. Commun.* **2013**,

49, 5480.
[34] S. Alberti, G. J. A. A. Soler-Illia, O. Azzaroni, *Chem. Commun.* **2015**, *51*, 6050–6075.
[35] L. Polo, N. Gómez-Cerezo, E. Aznar, J.-L. Vivancos, F. Sancenón, D. Arcos, M. Vallet-Regí, R. Martínez-Máñez, *Acta Biomater.* **2017**, *50*, 114–126.
[36] H. Bull, P. G. Murray, D. Thomas, A. M. Fraser, P. N. Nelson, *Mol. Pathol.* **2002**, *55*, 65–72.
[37] N. Mas, D. Arcos , L. Polo, E. Aznar, S. Sánchez-Salcedo, F. Sancenón, A. García, M.D. Marcos, A. Baeza, M. Vallet-Regí, R. Martínez-Máñez, *Small*, **2014**, *10*, 4859–4864.
[38] C. P. Price, A. Kirwan, C. Vader, *Calcif. Tissue Int.* **1982**, *34*, 285–290.
[39] L. J. Raggatt, N. C. Partridge, *J. Biol. Chem.* **2010**, *285*, 25103–8.
[40] J. A. Wright, S. P. Nair, *Int. J. Med. Microbiol.* **2010**, *300*, 193–204.
[41] L. L. Hench, *J. Am. Ceram. Soc.* **1991**, *74*, 1487–1510.
[42] T. Higuchi, *J. Pharm. Sci.* **1961**, *50*, 874−875.
[43] T. Higuchi, *J. Pharm. Sci.* **1963**, *52*, 1145−1149.
[44] E. Aznar, F. Sancenón, M.D. Marcos, R. Martínez-Máñez, P. Stroeve, J. Cano, P. Amorós, *Langmuir* **2012**, *28*, 2986−2996.
[45] R. Mathew, C. Turdean-Ionescu, B. Stevensson, I. Izquierdo-Barba, A. García, D. Arcos, M. Vallet-Regí, M. Edén, *Chem. Mater.* **2013**, *25*, 1877–1885.
[46] S. Brunauer, P. H. Emmett, E. Teller, *J. Am. Chem. Soc.* **1938**, *60*, 309–319.
[47] E. P. Barrett, L. G. Joyner, P. P. Halenda, *J. Am. Chem. Soc.* **1951**, *73*, 373–380.